JEE Journal of Ecological Engineering

Journal of Ecological Engineering, 2026, 27(2), 451–461
https://doi.org/10.12911/22998993/211775
ISSN 2299–8993, License CC-BY 4.0

Received: 2025.09.30
Accepted: 2025.12.15
Published: 2026.01.15

Adsorption efficiency of hydrogen sulfide using coconut shell-derived activated carbon and iron oxide composites

Pham Van Toan[1*], Tran Minh Vien[1], Hui Lin Ong[2]

[1] Department of Environmental Engineering, Can Tho University, Can Tho City 94000, Vietnam
[2] Faculty of Chemical Engineering & Technology, University Malaysia Perlis, 02600 Arau, Perlis, Malaysia
* Corresponding author's email: pvtoan@ctu.edu.vn

ABSTRACT

Hydrogen sulfide (H_2S) is a toxic gas commonly released from industrial activities, wastewater treatment, and biogas production, posing serious risks to human health and the environment. This study evaluated the adsorption efficiency of H_2S using coconut shell-derived activated carbon (AC) and iron oxide (FO). A series of experiments were conducted on a continuous laboratory scale adsorption column to examine the effects of adsorbent dosage, contact time, gas flow rate, and mixing ratio. The study results revealed a highest H_2S adsorption efficiency at the experiment conditions of 1 g material dosage, 60 min adsorption time, 500 $mL.min^{-1}$ gas flow rate, initial H_2S concentration of 70 ppm, and a mixing ratio of AC:FO = 70:30. The Thomas and Adams-Bohart models were applied to simulate the adsorption process. The Adams-Bohart model indicated that FO had a higher maximum adsorption capacity per unit volume (87.57 $mg.L^{-1}$ versus 7.55 $mg.L^{-1}$ for AC), suggesting a stronger initial adsorption ability. Further research on the effectiveness of the absorbents under real conditions are necessary.

Keywords: activated carbon, continuous adsorption, hydrogen sulfide, iron oxide.

INTRODUCTION

Air pollutants originating from hazardous organic and inorganic compounds have emerged as one of the most urgent environmental problems of the 21st century. These pollutants seriously impact public health, ecosystems, and sustainable development. Among toxic gases, hydrogen sulfide (H_2S) is particularly dangerous due to its characteristics as a colorless, flammable gas with a distinct rotten egg odor. H_2S is commonly generated from industrial processes such as petroleum refining, natural gas processing, paper production, and wastewater treatment (Blatt et al., 2014; Georgiadis et al., 2020). The release of H_2S into the environment not only contributes to air pollution but also poses severe risks to human health. H_2S can be detected at very low concentrations (4.7 $mg.m^{-3}$) in the ambient environment. Additionally, H_2S tends to accumulate, posing significant threats to worker safety and contributing to the corrosion of industrial equipment (D'Alessandro and Kyriakopoulos, 2013). Given these problems, reducing H_2S emissions in production is essential not only for compliance with increasingly stringent environmental regulations but also for preventing corrosion, extending equipment lifespan, and reducing maintenance costs. Various technologies have been developed for H_2S removal, including chemical absorption, biological treatment, photocatalysis, and precipitation. Among these technologies, adsorption using solid sorbents is considered the most favorable due to its low capital and operational costs, high regeneration potential, and effective performance at trace concentrations, especially when using locally available, environmentally friendly adsorbents (Georgiadis et al., 2020; Lau et al., 2018).

Activated carbon (AC) is one of the most extensively studied adsorbents due to its microporous structure and large specific surface area. Ling et al. (2019) reported that coconut shell-derived activated carbon can achieve a surface area exceeding 1.200 $m^2.g^{-1}$ after steam activation, with an average H_2S adsorption capacity ranging from 50 to 100 $mg.g^{-1}$ depending on pH

and temperature. Lau et al. (2018) found that surface treatment of AC with NaOH or metal compounds can enhance the H_2S adsorption capacity by 20–30% compared to untreated AC. However, pristine AC has the disadvantage of rapid saturation of adsorption locations, leading to a decline in performance after multiple regeneration cycles. In contrast, ferrous oxides (FO), particularly Fe_2O_3, are known for their chemical adsorption of H_2S, forming Fe_2S_3 and elemental sulfur on the sorbent surface, effectively preventing re-release of H_2S under pressure drops. Georgiadis et al. (2020) demonstrated that Fe_2O_3 synthesized via hydrothermal and precipitation methods with nanoparticle sizes ranging between 14–21 nm, can achieve adsorption capacities of 100–150 $mg.g^{-1}$. Moreover, their reusability was maintained across multiple cycles through surface oxidation regeneration. However, due to their limited surface area (typically smaller 100 $m^2.g^{-1}$) and lack of micropores, the diffusion rate of H_2S into ferrous oxide particles is lower than that in AC.

To overcome the limitations of above individual materials and to leverage the advantages of both, a promising approach involves blending AC with FO or producing AC-FO nanocomposites. Blatt et al. (2014) produced Fe_2O_3-AC composites via thermal spraying, resulting in uniformly dispersed Fe_2O_3 nanoparticles (approx. 7.5 nm) on a carbon framework, achieving a surface area of approximately 150 $m^2.g^{-1}$, tripling the H_2S adsorption capacity compared to directly Fe_2O_3 impregnated AC. Ling et al. (2019) also demonstrated that a mixture of coconut shell-derived AC and Fe_2O_3 could reach an H_2S adsorption capacity exceeding 200 $mg.g^{-1}$, with the adsorption kinetics fiting the Langmuir model. However, most previous studies have focused on AC or FO individually, with limited comprehensive assessments of their mixtures at varying blend ratios. There remains a gap in optimizing operational parameters such as sorbent mass, gas flow rate, retention time, and mixing ratio. Addressing this gap requires systematic research to determine optimal operating conditions for AC-FO mixtures and to elucidate their combined physico-chemical adsorption mechanisms. Therefore, this study aims to (1) determine optimal adsorption conditions (adsorbent dosage, gas flow rate, retention time, and AC:FO mixing ratio) and (2) apply the Thomas and Adams-Bohart kinetic models for estimating the adsorption capacity (q) of the adsorbents. The findings are expected to provide a scientific foundation for the effective application of AC-FO composite materials in H_2S gas treatment, in compliance with increasingly rigorous environmental standards.

MATERIALS AND METHODS

Materials and chemicals

The H_2S gas used in the study was 99% pure, stored in 60-liter steel cylinders manufactured in the Vietnam. The adsorbents included coconut shell activated carbon with a particle size of 0.07–4.76 mm, bulk density ranging from 0.44 to 0.6 $g.cm^{-3}$, and an H_2S adsorption index of 1.100 $mg.g^{-1}$; and pelletized iron oxide in cylindrical form with a length ranging from 20 to 30 mm, diameter of 5–6 mm, bulk density of 5.24 $g.cm^{-3}$, and an H_2S adsorption index of 700–800 $mg.g^{-1}$.

Adsorption system model

The experimental system was designed to investigate the H_2S adsorption capabilities of various materials under controlled laboratory conditions. The system enabled precise determination of H_2S removal efficiency by comparing gas concentrations before and after exposure to the adsorbents. To enhance statistical reliability, each treatment was conducted simultaneously using three identical adsorption columns.

Initially, H_2S gas (denoted as A in the Figure 1 was introduced via a regulating valve into the first gas mixing chamber (GM1), where it was blended with air supplied by blower AB1. This produced a primary gas stream containing H_2S. Since the H_2S concentration after GM1 often exceeded the target level, further dilution was performed the second gas mixing chamber (GM2), where additional dilution occurs using air from blower AB2. The two-stage mixing allowed flexible and precise control of inlet H_2S concentration, ensuring consistency across repetitions and different treatments. After mixing, the gas flow passes through a flow meter (FM) for monitoring and adjustment before being equally distributed into three parallel adsorption columns, each containing a specific adsorbent. Inlet gas sampling valves (IG1, IG2, IG3) are installed on the gas lines feeding the columns to collect samples and measure H_2S concentrations prior to adsorption. During the process, H_2S gas flowed through the

Symbol	Description
A	H_2S gas
AB1	Air blower 1
AB2	Air blower 2
OG1	Outlet gas 1
OG2	Outlet gas 2
OG3	Outlet gas 3
FM	Flow meter
GM1	Gas mixer 1
GM2	Gas mixer 2
IG1	Inlet gas 1
IG2	Inlet gas 2
IG3	Inlet gas 3
	Control valve

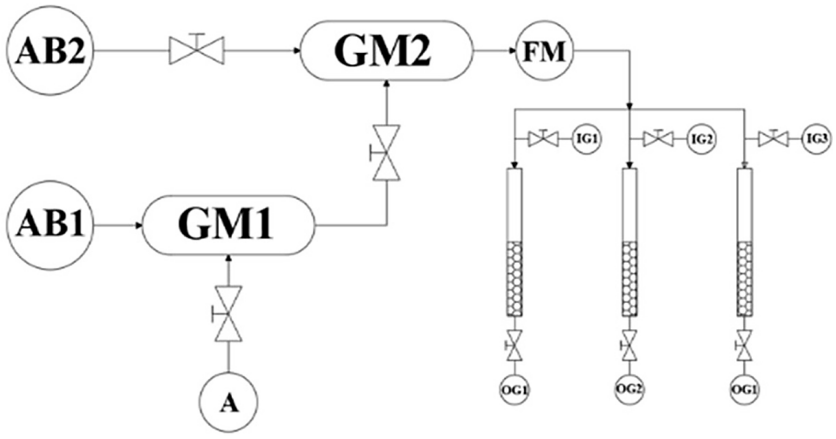

Figure 1. Scheme of H_2S adsorption system model

adsorbent beds in cylindrical tubes, where physical and/or chemical adsorption occurred on the surface and within the pore network of the materials, resulting in decreased H_2S concentration. The use of three identically operated columns facilitates control over measurement accuracy, material homogeneity assessment, and system stability evaluation. Finally, the treated gas exited the columns through outlet sampling valves (OG1, OG2, OG3), where post-adsorption gas samples were collected to determine residual H_2S concentrations. The concentration difference between inlet (IG) and outlet (OG) samples was used to calculate the adsorption efficiency.

Experimental design

Experiments were conducted to evaluate the effects of operational parameters on the H_2S adsorption performance. Parameters included absorbent mass, contact time, gas flow rate, and AC:FO mixing ratios. The parameter selection was based on previous studies (Choo, et al., 2013; Zulkefli, et al., 2022) and modified to suit the experimental setup.

Effect of absorbent mass

Adsorbents at five different weights (4 g, 5 g, 6 g, 7 g, and 8 g) for each material type, with other conditions held constant: contact time of 60 min, gas flow rate of 400 $mL.min^{-1}$, and inlet H_2S concentration of 70 ppm (97.6 $mg.m^{-3}$). Each experiment was repeated three times.

Effect of contact time

Thirteen contact time intervals (5 to 480 min) were tested for each material, using the optimal mass result obtained from the experiment on the effect of absorbent mass. Other parameters included a gas flow rate of 400 $mL.min^{-1}$ and inlet H_2S concentration of 70 ppm were fixed. Each experiment was repeated three times.

Effect of gas flow rates

Five gas flow rates (300 $mL.min^{-1}$, 400 $mL.min^{-1}$ 500 $mL.min^{-1}$, 600 $mL.min^{-1}$, and 700 $mL.min^{-1}$) were tested, using the optimal mass and contact time obtained from the experiment on the effect of absorbent mass and contact time. The H_2S concentration remained at 70 ppm. Each experiment was repeated three times.

Effect of AC:FO mass ratio

Five AC:FO mass ratios (100:0, 70:30, 50:50, 30:70, and 0:100) were tested, using the optimal mass, contact time, and flow rate obtained from above experiments, at inlet H_2S concentration of 70 ppm. Each experiment was conducted in triplicate.

Determination of H_2S concentration

H_2S concentrations were determined using a GA5000 gas analyzer (Geotech, UK). For each experiment, after the gas passing adsorption system reached a stable volume for approximately 2 min, inlet gas samples were collected in a polyethylene (PE) zipper bags and analyzed using a GA5000 gas analyzer. Post-adsorption samples were collected and analyzed similarly. The H_2S concentrations were displayed directly on the device's LCD screen.

Evaluation of adsorption process

Adsorption efficiency

H_2S adsorption capacity (q, mg.g^{-1}) and adsorption efficiency (H, %) were calculated using fomula (Equation 1) and (Equation 2) (Saleh et al., 2024).

$$q = \frac{(C_0 - C_e) \times V}{m} \quad (1)$$

$$H = \frac{(C_0 - C_e)}{C_0} \quad (2)$$

where: C_0 and C_e are the initial and final H_2S concentrations (mg.m^{-3}), respectively, V is the gas volume (m^3), and m is the mass of the adsorbent (g).

Kinetic models

The study of the adsorption process in a continuous column system often requires the application of kinetic models to describe and analyze the efficiency of the adsorbent. These models allow assessment of pollutant removal capability, optimal operating time, and determination of important parameters such as adsorption capacity, reaction rate, and saturation point. Two commonly used models in adsorption kinetics are the Thomas model and the Adams-Bohart model.

The Thomas model is the most widely used in column-typed adsorption studies. The maximum concentration of the adsorbed substance in the solid phase on adsorbent's surface and the rate constant were determined based on data collected from continuous adsorption studies in columns. The Thomas equation is expressed in linear form (Equation 3) (Saleh et al., 2024).

$$ln\left(\frac{C_0}{C_t} - 1\right) = \frac{k_{Th} q_0 m}{Q} - k_{Th} C_0 t \quad (3)$$

where: C_0 and C_t are the initial and time t concentrations of H_2S (mg.m^{-3}); k_{Th} is the Thomas model rate constant (L.min^{-1}.mg^{-1}); q_0 is the maximum adsorption capacity (mg.g^{-1}); m is the mass of the adsorbent (g); Q is the gas flow rate (mL.min^{-1}); t is the adsorption time (min). The values of k_{Th} and q_0 can be determined from the linear plot of $\ln(C_0/C_t - 1)$ versus time t.

The Adams-Bohart model describes the initial stage of the adsorption process in a column, when the pollutant concentration remains high and the adsorbent is not yet saturated. This model assumes that the adsorption rate is proportional to the influenced concentration and is unaffected by efficiency reduction at this stage. The Adams-Bohart equation is expressed in linear form (Equation 4) (Saleh et al., 2024).

$$ln\left(\frac{C_0}{C_t}\right) = k_{AB} C_0 t - \frac{k_{AB} N_0 Z}{F} \quad (4)$$

where: k_{AB} is the Adams-Bohart model rate constant (L.min^{-1}.mg^{-1}); N_0 is the maximum volumetric sorption capacity of the adsorbent (mg.L^{-1}); Z is the bed thickness of the material in the column (cm); and F is the linear velocity (cm.min^{-1}), calculated by dividing the flow rate by the column area.

Both models provide important theoretical foundations for analyzing adsorption kinetics in column systems, supporting the design and optimization of operational parameters in adsorption processes.

Data analysis

Experimental data were statistically analyzed using IBM SPSS Statistics version 26 software. One-way ANOVA was applied to test differences among adsorption process parameters, followed by Duncan test at a 5% significance level. Normality and homogeneity of variance were verified prior to analysis to ensure the appropriate test method was selected.

RESULTS AND DISCUSSION

Effect of factors on H_2S adsorption capacity

Effect of adsorbent mass

Adsorbent mass is one of the critical parameters influencing the removal efficiency of H_2S from the gas stream. To evaluate this factor, experiments were conducted using five different mass levels (4 g, 5 g, 6 g, 7 g, and 8 g) for both coconut shell-based activated carbon (AC) and iron oxide (FO). Other experimental conditions were kept constant, including an H_2S gas flow rate of 400 mL.min^{-1}, an initial H_2S concentration of 70 ppm, and a contact time of 60 minutes. Experiment results show that the outlet H_2S concentration decreased with increasing adsorbent mass from 0.93 ± 0.46 mg.m^{-3} at 4–6 g of AC to 0.46 ± 0.46 mg.m^{-3} at 7–8 g. FO

followed a similar trend, with the outlet concentration decreasing from 1.86 ± 0.46 mg.m^{-3} (4 g) to 0.46 ± 0.46 mg.m^{-3} (6 g). However, statistical analysis showed no significant differences in outlet H_2S concentrations across the tested (AC: p = 0.939; FO: p = 0.225).

The H_2S removal efficiency increased slightly with increasing adsorbent mass, from 98.67 % (4 g) to 99.33 % (8 g) for AC, and from 97.33 % (4 g) to 99.33 % (6 g) for FO. This improvement can be attributed to the greater surface area and number of adsorption sites available for adsorption, consistent with findings in Juma et al. (2020). Nevertheless, the differences in efficiency among treatments were not statistically significant (AC: p = 0.940; FO: p = 0.226).

When considering the amount of H_2S adsorbed per gram of adsorbent (q, mg.g^{-1}), q decreased from 0.33 mg.g^{-1} to 0.15 mg.g^{-1} for AC and from 0.4 mg.g^{-1} to 0.21 mg.g^{-1} for FO as the adsorbent mass increased from 4 g to 8 g (Figure 2). This inverse relationship is attributed to the "shielding effect", where upper layers of the adsorbent hinder access to the adsorption sites in lower layers, thereby reducing the H_2S adsorption efficiency (Juma et al., 2020). Statistical analysis confirmed significant differences in specific adsorption capacity among the tested mass levels (p = 0.008), with the 4 g mass yielding the highest adsorption capacity value. Although the 4 g adsorbent demostrated the highest specific adsorption capacity, the time required to reach saturation remained relatively long. For instance, Zulkefli et al. (2022) reported that 150 g of AC, took 250–300 min to reach saturation at an H_2S concentration of 5.000 ppm. Therefore, for a lower concentration of 70 ppm, reducing the adsorbent mass to 1 g is considered reasonable to shorten the experimental time to accelerate equilibrium attainment and streamline experimental duration. Based on this, 1 g of adsorbent was selected for subsequent experiments to optimize the balance between H_2S removal efficiency, adsorption capacity, and operational time under the defined experimental conditions.

Effect of contact time

Contact time plays a critical role in achieving adsorption equilibrium and maximizing the H_2S adsorption capacity by adsorbent. To identify the optimal duration, experiments were conducted with an adsorbent amount of 1 g, an initial H_2S concentration of 70 ppm, a gas flow rate of 400 mL.min^{-1}, and contact times ranging from 5 to 480 min.

For AC, no detectable H_2S was observed in the outlet stream during the initial 5–30 min, indicating complete adsorption. Beyond 60 min, outlet concentrations gradually increased from 0.46 ± 0.8 mg.m^{-3} (60 min) to 25.09 ± 3.69 mg.m^{-3} (480 min). Statistical analysis revealed no significant differences in outlet concentrations between 5 to 120 min, whereas a marked increase was observed from 180 min onwards (p = 0.000). In contrast, FO exhibited detachable H_2S from the outlet with rapid concentration rising 6.97 ± 0.0 mg.m^{-3} (5 min), followed by a steadily rose to 40.89 ± 1.61 mg.m^{-3} at 480 min, with significant differences across all time points (p = 0.000).

The adsorption capacity (q) of AC increased rapidly from 0.14 mg.g^{-1} (5 min) to 7.77 mg.g^{-1} (300 min), reaching near saturation at 360–480 min (8.59–8.70 mg.g^{-1}) (Figure 3). FO followed a similar trend but at a slower rate, with q_t increasing from 0.13 mg.g^{-1} (5 min) to 5.11 mg.g^{-1} (300 min) and saturating at 360–480 min (5.73–6.04 mg.g^{-1}). The rapid q increase in the initial stage indicates abundant active sites on the adsorbent surface facilitating efficient fast H_2S adsorption. As contact time extended, these active sites became saturated reducing the driving force and rate of adsorption, which led to performance decline and saturation Le et al., (2018).

AC's adsorption capacity maintained at 100% removal efficiency during the first 5–30 min, dropping to 59.38% at 480 min. FO's adsorption capacity started at 90.32% (5 min) and decreased to 43.59% at 480 min. Differences in performance among contact times during the first 5–30 min is no significant but became statistically significant after 180 min (p = 0.000) for both adsorbents.

Experiment results show that the maximum adsorption efficiency was observed at the first 5 min, but the H_2S adsorption capacity was still low indicating incomplete adsorption. Although maximum adsorption capacity was achieved at 480 minutes, the corresponding efficiency was substantially lower. Conversely, at 60 min, both adsorbents demonstrated a balance between adsorption efficiency and capacity: AC achieved 99.37% adsorption efficiency and 3.27 mg.g^{-1} capacity; while FO reached 81.95% adsorption efficiency and 3.05 mg.g^{-1} capacity. These values were statistically different from longer durations

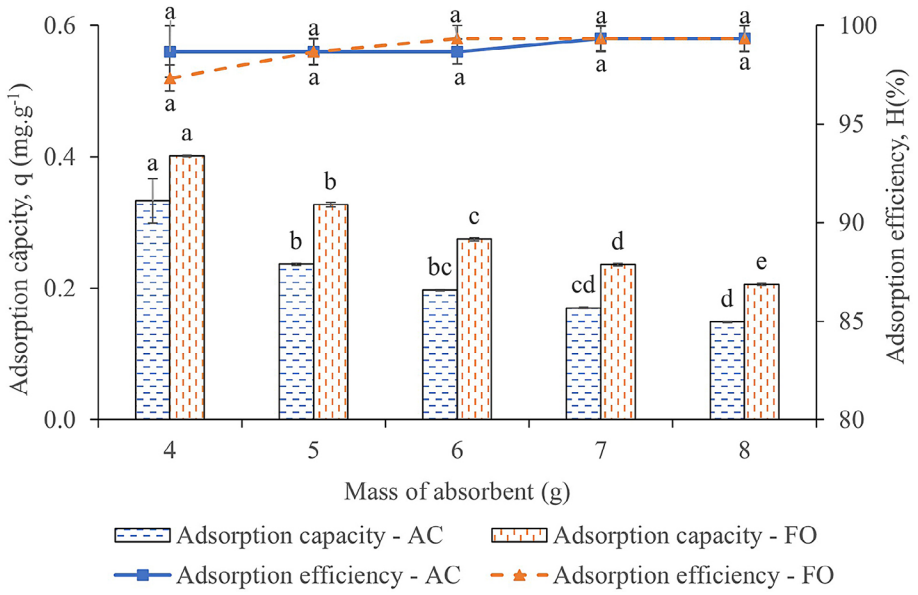

Figure 2. H_2S removal efficiency per unit mass of AC and FO. Concentrations are presented as mean ± standard deviation (n=3). Different letters indicate statistically significant differences at the level of 5%

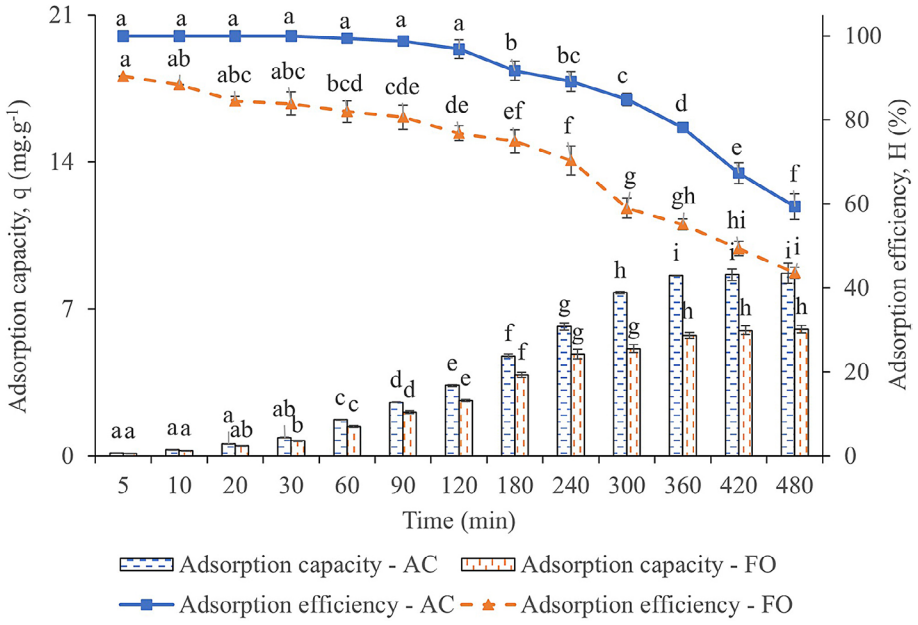

Figure 3. Effect of contact time on the H_2S adsorption capacity of two materials. Values are presented as mean ± standard deviation. Different letters indicate statistically significant differences at the level of 5%

(p = 0.000) but not significantly different from shorter times.

Based on these findings, a contact time of 60 min was selected for subsequent experiments, offering an optimal compromise between adsorption efficiency, capacity, and experimental practicality.

Effect of gas flow rate

Gas flow rate directly influences the contact time between H_2S molecules and the adsorbent surface, thereby affecting both adsorption efficiency and capacity. To investigate the effect of this parameter, experiments were conducted at five flow rates such as 300, 400, 500, 600, and 700 mL.min^{-1}, with a fixed adsorbent mass of 1 g, contact time of 60 min, and initial H_2S concentration of 70 ppm.

Experiment results showed a clear increase in outlet H_2S concentration with increasing flow rate. For activated carbon (AC), H_2S was

undetectable at 300 mL.min^{-1} but increased to 1.40 ± 1.39 mg.m^{-3} (400 mL.min^{-1}), 4.18 ± 3.69 mg.m^{-3} (500 mL.min^{-1}), 6.97 ± 0.0 mg.m^{-3} (600 mL.min^{-1}), and peaked at 11.62 ± 3.21 mg.m^{-3} (700 mL.min^{-1}). For iron oxide (FO), initial concentrations were 6.50 ± 2.90 mg.m^{-3} at 300 mL.min^{-1}, increasing to 13.4 ± 2.13; 16.73 ± 1.39; 26.02 ± 4.48; and 28.81 ± 1.61 mg.m^{-3} at gas flow rates 400; 500; 600 và 700 mL.min^{-1}, respectively. Statistical analysis confirmed significant differences in outlet concentrations among flow rates for both materials (AC: p = 0.016; FO: p = 0.000).

Adsorption capacity per gram of material increased with flow rate (Figure 4). For AC, adsorption capacity rose from 1.33 mg.g^{-1} (300 mL.min^{-1}) to 2.67 mg.g^{-1} (700 mL.min^{-1}). FO showed a slower increase from 1.25 mg.g^{-1} (300 mL.min^{-1}) to 1.91 mg.g^{-1} (700 mL.min^{-1}); saturation appeared around 500 mL.min^{-1}, with little change at 600 and 700 mL.min^{-1} indicating FO's limited adsorption capacity at higher flow rates. FO began to reach saturation at a gas flow rate of 500 mL.min^{-1}, with an H_2S adsorption capacity of 1.72 mg.g^{-1}, while the AC material continued to increase its adsorption capacity. This difference primarily arises from the distinct mechanisms and structural characteristics of the two materials. Specifically, FO adsorbs H_2S through an irreversible chemical reaction, forming products such as FeS_2, Fe_3S_4, and elemental sulfur. These products permanently occupy active sites, causing the material to rapidly reach saturation as the gas flow rate increases. Ling et al. (2019) reported that H_2S mainly reacts on the surface of Fe_2O_3, with slow diffusion through the crystal lattice, thereby limiting the effective adsorption region within the material particles. In contrast, AC adsorbs H_2S primarily via physical adsorption, which depends on its large surface area and abundant microporous network, allowing gas molecules to diffuse deeply into the pore structure even at high flow rates.

It could see that H_2S adsorption efficiency decreased markedly with increased gas flow rate. Specifically, AC's adsorption efficiency maintained 100% at 300 mL.min^{-1}, dropped to 98.10% (400 mL.min^{-1}), 94.55% (500 mL.min^{-1}), 90.62% (600 mL.min^{-1}), and 84.60% (700 mL.min^{-1}). FO's efficiency declined from 91.51% (300 mL.min^{-1}) to 61.26% (700 mL.min^{-1}). At lower gas flow rates, longer contact time allows deeper H_2S diffusion into pores and stronger interaction with material. Conversely, at higher gas flow rates, reduced contact time limits diffusion and active site interaction (Juma et al., 2020; Zulkefli et al., 2017).

In summary, at 500 mL.min^{-1}, AC reached 94.55% for efficiency and 2.16 mg.g^{-1} for adsorption capacity, outperforming FO (77.49% and 1.72 mg.g^{-1}) with statistical significance. Thus, gas flow rate of 500 mL.min^{-1} was chosen as the

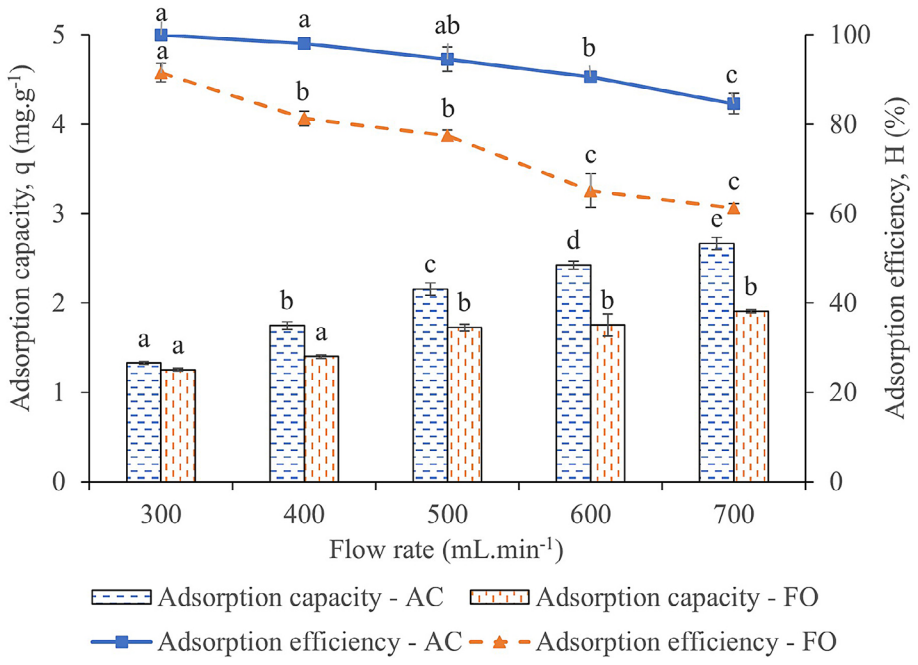

Figure 4. Effect of gas flow rate on the H_2S adsorption. Values are presented as mean ± standard deviation (n = 3). Different letters indicate statistically significant differences at the level of 5%

optimal balance between adsorption efficiency and capacity, reinforcing the superior surface area and pore structure of AC in H_2S adsorption.

Effect of mixing ratios

Experiments were conducted to determine the optimal mixing ratio of activated carbon (AC) and iron oxide (FO) for H_2S gas adsorption. Experiment conditions included a total adsorbent mass of 1 g, contact time of 60 min, gas flow rate of 500 mL.min^{-1}, and an initial H_2S concentration of 70 ppm. Five mass ratios of AC:FO consisting of 100:0; 70:30; 50:50; 30:70; 0:100 were tested in triplicate.

Experiment results show that H_2S outlet concentration increased as the FO ratio increased. Specifically, pure AC (100:0) yielded the lowest H_2S outlet concentration (5.11 ± 0.80 mg.m^{-3}) while pure FO (0:100) had the highest H_2S outlet concentration (11.62 ± 0.80 mg.m^{-3}). Three intermediate ratios showed H_2S outlet concentrations of 5.58 ± 2.41 mg.m^{-3} (70:30); 7.43 ± 1.61 mg.m^{-3} (50:50); and 10.22 ± 0.80 mg.m^{-3} (30:70). Statistical testing confirmed differences at the significant level of 5% among the mixing ratio ($p = 0.003$).

Adsorption efficiency of H_2S decreased from 93.08% (100:0) to 84.38% (0:100) as FO content increased, with intermediate efficiencies of 89.67% (70:30); 86.25% (50:50); and 84.38% (30:70) (Figure 5). Treatments were statistically divided into three distinct efficiency groups: the highest one (100%AC), the medium (70:30; 50:50; 30:70); and the lowest (100%FO) ($p = 0.025$).

Adsorbed gas H_2S amount followed the trend with increase of the FO ratio, decreasing from 2.06 mg.g^{-1} (100:0) to 1.87 mg.g^{-1} (0:100); with intermediate values of 1.97 mg.g^{-1} (70:30); 1.93 mg.g^{-1} (50:50); and 1.91 mg.g^{-1} (30:70). The differences in adsorption capacity across the mixing ratios were statistically significant ($p = 0.005$), and similar to adsorption efficiency trends.

Based on comparisons between adsorption efficiency and capacity, a 70:30 (AC:FO) ratio was identified as an optimal mixing ratio. At this ratio, AC remained dominant in adsorption performance (92.23%) and statistically equivalent to pure AC. FO plays a supplementary role through an irreversible chemical adsorption mechanism, which immobilizes H_2S on the surface in the form of compounds such as FeS_2 or elemental sulfur. This mechanism contributes to enhanced adsorption stability and reduces the risk of re-desorption, compared to AC, which primarily relies on physical adsorption and is more susceptible to variations in operating conditions. Fauteux-Lefebvre et al. (2015) confirmed that combining metal oxides with activated carbon can significantly improve H_2S removal efficiency through a chemical reaction mechanism. Moreover, thus mixing ratio reduces material cost and volume compared to using only activated carbon (Juma et al., 2020).

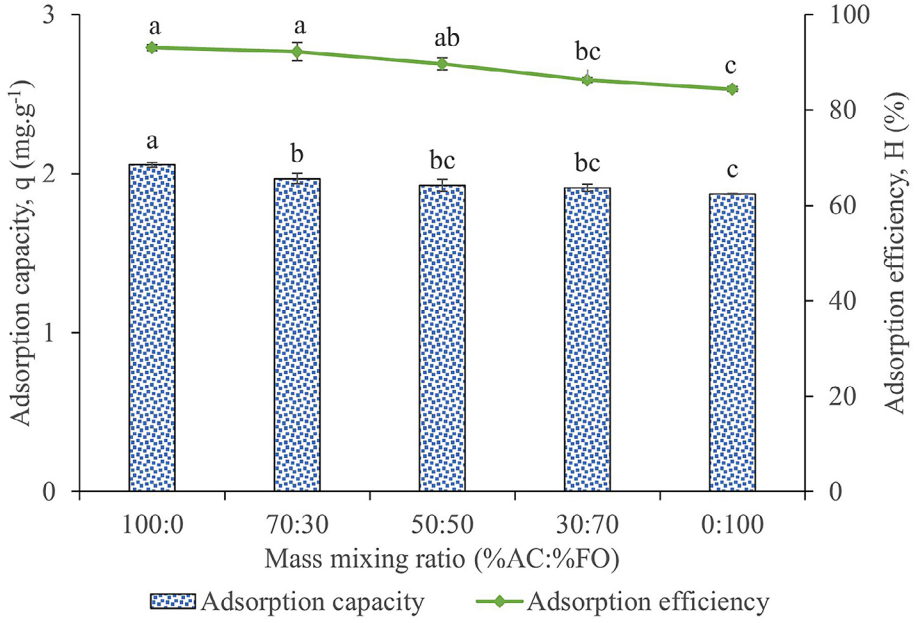

Figure 5. Effect of material mixing ratio on the H_2S adsorption capacity. Values are presented as mean ± standard deviation (n=3). Different letters indicate statistically significant differences at the level of 5%

Adsorption kinetic models

Thomas model

The Thomas kinetic model was applied to analyze the H_2S adsorption process under continuous flow conditions with two different adsorbent materials AC and FO. Two key parameters obtained from the model including the Thomas rate constant (k_{Th}) and maximum adsorption capacity (q_0) showed a significant difference between the two materials.

Activated coconut shell carbon had a k_{Th} value of 0.1513 $L.mg^{-1}.min^{-1}$, nearly 2.2 times higher than FO (0.0686 $L.mg^{-1}.min^{-1}$) indicating a significantly higher initial adsorption rate of AC. This reflects the rapid reaction capability of AC with H_2S molecule enhancing treatment efficiency in a short time. Additionally, the maximum adsorption capacity of AC reached 13.08 $mg.g^{-1}$, superior to FO (10.99 $mg.g^{-1}$). This result may be related to rich microporous structure and large specific surface area for AC, especially when produced from coconut shells. Experimental data of the effect of contact time also supports this conclusion: AC only began to show H_2S in the outlet stream after 60 min, while FO exhibited early breakthrough from the 5th minute. This confirms a longer and more effective adsorption performance of AC in continuous flow. The correlation coefficient R^2 of both materials was high (AC: 0.9344 and FO: 0.9682) indicating the Thomas model fitted with the experimental data (Figure 6). Although FO showed a better fit with the mathematical model, the kinetic indicators and actual efficiency demonstrated advantage of AC in both speed and adsorption capacity.

In sum, AC demonstrated superior adsorption capability both in terms of kinetics and capacity while FO showed higher modeling stability. Depending on application goals whether prioritizing fast and efficient treatment (for AC) or requiring high model predictability and stability (for FO), each material has its own application potential in H_2S gas treatment.

Adams-Bohart model

The Adams-Bohart kinetic model was applied to describe the initial stage of the adsorption process in the column system, assuming that the adsorption rate is proportional to the initial pollutant concentration and the number of available adsorption sites on the material surface. Linear regression allowed estimation of two key parameters rate constant (k_{AB}) and maximum adsorption capacity density (N_0) of the material under initial flow conditions.

Coconut shell-derived activated carbon (AC) reached a k_{AB} value of 0.1327 $L.mg^{-1}.min^{-1}$, significantly higher than FO material (0.0473 $L.mg^{-1}.min^{-1}$). This indicates that AC has a higher initial adsorption rate due to its rapid access to H_2S molecule thanks to its large surface area and

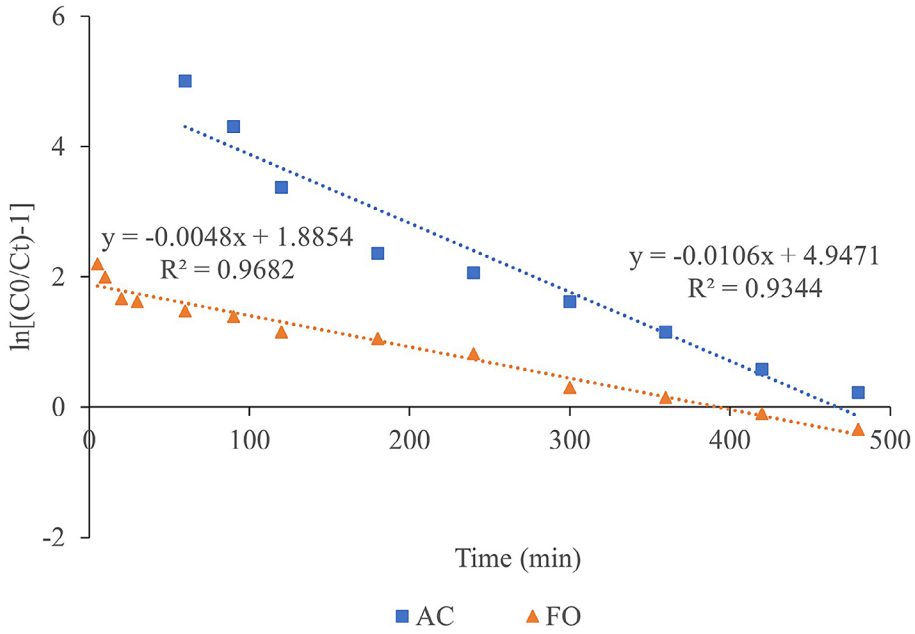

Figure 6. Thomas kinetic model for AC and FO adsorbents

favorable pore structure (Ling et al., 2019). However, the N_0 value of FO was more remarkable, reaching 87.574 mg.L^{-1}, nearly 11 times higher than AC (7.549 mg.L^{-1}). This difference indicates that FO can retain a larger amount of H_2S from the beginning, possibly due to a high density of adsorption sites or favorable interactions between H_2S and present of iron oxide in the material.

Both materials showed good compatibility to model experiment, with R^2 values of 0.9016 for AC and 0.9374 for FO (Figure 7). The regression linear of FO showed a higher degree of fit indicating that the Adams-Bohart model describes initial adsorption kinetic for FO more accurately than AC.

Based the analysis results it could be concluded that AC has an advantage in initial treatment speed while FO has greater H_2S retention ability in the early stage. These two materials represent two different adsorption processes: AC is suitable for systems requiring rapid pollutant removal, while FO is suitable for applications requiring high processing capacity over a long duration.

Comparison between Thomas and Adams-Bohart models

Both Thomas and Adams-Bohart models are widely used in adsorption studies under continuous flow conditions, but each reflects a different kinetic aspect. The Thomas model is based on the Langmuir isotherm assumption and assumes no chemical reaction. It is suitable for describing the entire adsorption process. Conversely, the Adams-Bohart model mainly reflects the initial stage of the process where the reaction rate strongly depends on the initial concentration and the number of available adsorption sites.

Study results show that, according to the Thomas model, activated carbon had higher kinetic parameters including the rate constant (k_{Th}) and maximum capacity (q_0), indicating the ability to treat H_2S quickly and efficiently during the entire of operation. On the other hand, the Adams-Bohart model showed that FO material had a significantly higher initial saturation density (N_0) although the initial adsorption rate (k_{AB}) was lower, implying that FO had strong adsorption capability in the initial stage due to structural characteristics or specific chemical interactions with H_2S. Regarding model fit, both materials had correlation coefficients above 0.9 indicating good fit with experimental data. However, FO showed higher model consistency especially with the Adams-Bohart model indicating more stable kinetics in the initial adsorption stage.

In general, the Thomas model provides a comprehensive view of adsorption efficiency over time, suitable for predicting material behavior under extended operation. Meanwhile the Adams-Bohart model provides useful information on instantaneous adsorption mechanisms. Therefore, the choice of model and adsorbent material

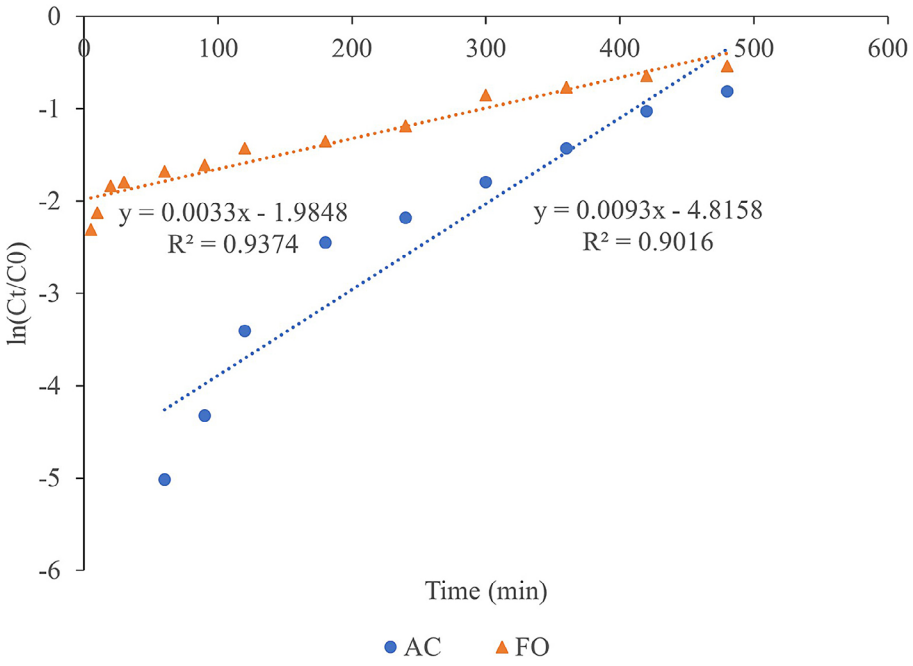

Figure 7. Adams-Bohart kinetic model for AC and FO adsorbents

should be considered based on specific application objectives whether prioritizing fast treatment or high initial adsorption capacity.

CONCLUSIONS

Activated coconut shell carbon and iron oxide demonstrated high effectiveness in removing H_2S. Efficiency of H_2S adsorption was identified at 1 g material dosage, 60 min adsorption time, 500 $mL.min^{-1}$ gas flow rate, initial H_2S concentration of 70 ppm, and a mixing ratio of AC:FO = 70:30. Kinetic modeling results for Thomas and Adams-Bohart models well fitted with experimental data ($R^2 > 0.9$). The Thomas model emphasized the superior performance of AC (k_{Th} = 0.1513 $L.mg^{-1}.min^{-1}$; q_0 = 13.08 $mg.g^{-1}$), while the Adams-Bohart model highlighted FO's high initial adsorption capacity. The study underscores the dominant role of AC in H_2S removal due to its extensive surface area and porosity, while FO remains crucial for reducing material volume and cost in systems with limited space.

Acknowledgements

This research was facilitated by the Air Pollution Control Lab. The authors express their sincere gratitude for valuable advice from the members of AGriCTU group – Can Tho University.

REFERENCES

1. Blatt, O., Helmich, M., Steuten, B., Hardt, S., Bathen, D., Wiggers, H. (2014). Iron Oxide/Polymer-based nanocomposite material for hydrogen sulfide adsorption applications. *Chemical Engineering & Technology*, *37*(11), 1938–1944. https://doi.org/10.1002/ceat.201400303
2. Choo, H. S., Lau, L. C., Mohamed, A. R., Lee, K. T. (2013). Hydrogen sulfide adsorption by alkaline impregnated coconut shell activated carbon. *Journal of Engineering Science and Technology*, *8*(6), 741–753.
3. D'Alessandro, W., Kyriakopoulos, K. (2013). Preliminary gas hazard evaluation in Greece. *Natural Hazards*, *69*(3), 1987–2004. https://doi.org/10.1007/s11069-013-0789-5
4. Fauteux-Lefebvre, C., Abatzoglou, N., Blais, S., Braidy, N., Hu, Y. (2015). Iron oxide-functionalized carbon nanofilaments for hydrogen sulfide adsorption: The multiple roles of carbon. *Carbon*, *95*, 794–801.
5. Georgiadis, A. G., Charisiou, N. D., Goula, M. A. (2020). Removal of hydrogen sulfide from various industrial gases: a review of the most promising adsorbing materials. *Catalysts*, *10*(5). https://doi.org/10.3390/catal10050521
6. Juma, G., Machunda, R., Pogrebnaya, T. (2020). Performance of sweet potato's leaf-derived activated carbon for hydrogen sulphide removal from biogas. *Journal of Energy*, 1–10. https://doi.org/10.1155/2020/9121085
7. Lau, L. C, Nor, N. M., Lee, K. T., Mohamed, A. R. (2018). Hydrogen sulfide removal using CeO_2/NaOH/PSAC: Effect of preparation parameters. *Journal of Environmental Chemical Engineering, 6*(1), 386–394. https://doi.org/10.1016/j.jece.2017.12.019
8. Le T. H., Le H. S., Nguyen, T. T. H., Pham, T. B., Nguyen, T. T. H., Nguyen, B. H., Ngo, N. T., Cu, T. N. (2018). Study on the potential use of activated carbon as an adsorbent material for H_2S gas. *Vietnam Journal of Agricultural Science and Technology*, *3*(88), 94–97.
9. Ling, K., Gangoli, V. S., & Barron, A. R. (2019). Synergic Adsorption of H_2S Using High Surface Area Iron Oxide–Carbon Composites at Room Temperature. *Energy & Fuels*, *33*(8), 7509–7521. https://doi.org/10.1021/acs.energyfuels.9b01012
10. Saleh, A. M., Mahdi, H. H., Alias, A. B., Abd Hadi, N. K., Qarizada, D., Jawad, A. H., Saleh, N. M. (2024). Equilibrium and kinetic studies in adsorption of H_2S using coconut shell activated carbon xerogel: Effect of mass adsorbent and temperature. *Desalination and Water Treatment*, *317*, 100149.
11. Zulkefli, N. N., Masdar, M. S., Isahak, W. R. W., Jahim, J., Majlan, E. H., Rejab, S. A. M., Lye, C. C. (2017). Mathematical modelling and simulation on the adsorption of Hydrogen Sulfide (H_2S) gas. *IOP Conference Series: Materials Science and Engineering*, *206*(1), 012069. https://iopscience.iop.org/article/10.1088/1757-899X/206/1/012069/meta
12. Zulkefli, N. N., Seladorai, R., Masdar, M. S., Mohd Sofian, N., Wan Isahak, W. N. R. (2022). Core shell nanostructure: Impregnated activated carbon as adsorbent for hydrogen sulfide adsorption. *Molecules*, *27*(3), 1145.